Journal of Pain Research

Dovepress
Taylor & Francis Group

Open Access Full Text Article

ORIGINAL RESEARCH

Electroacupuncture and Parecoxib Reduce Inflammatory Injury in a Primary Dysmenorrhea Rat Model: Investigating the Role of the COX-2/NF-κB/NLRP3 Pathway

Xiao Xue[1,2], Shaohua Wang[2], Juan Li[2], Hanyu Yuan[2], Sian Pan[2], Xin Liu[1], Zenghui Yue[2], Yu Liu[2]

[1]The First Affiliated Hospital, Department of Chinese Medicine, Hengyang Medical School, University of South China, Heng yang, Hunan, 421000, People's Republic of China; [2]College of Acupuncture, Massage and Rehabilitation, Hunan University of Chinese Medicine, Changsha, 410208, People's Republic of China

Correspondence: Zenghui Yue; Yu Liu, College of Acupuncture, Massage and Rehabilitation, Hunan University of Chinese Medicine, Changsha, 410208, People's Republic of China, Tel +86 13787293866; +86 – 15084947646, Fax +86 - 0731 – 88458189, Email yue5381316@126.com; luveyu@126.com

Purpose: Anti-inflammatory drugs relieve primary dysmenorrhea (PDM), and nucleotide-binding oligomerization domain-like receptor protein 3 (NLRP3) is a potential treatment target. Electroacupuncture (EA) is an effective alternative strategy for treating PDM as it regulates the NLRP3 inflammasome. However, the exact anti-inflammatory mechanism of EA remains unclear. Therefore, this study explored the therapeutic effect of EA on PDM and determined the potential involvement of the cyclooxygenase-2 (COX-2)/nuclear factor κB (NF-κB)/NLRP3 signaling pathway.

Patients and Methods: The following pain management interventions were administered to a PDM rat model: saline (control), EA, parecoxib, EA + parecoxib, or ibuprofen. After treatment, the following parameters were examined: torsion behavior; endometrial histopathological morphology and ultrastructure; serum and uterine prostaglandin E_2 (PGE_2) and prostaglandin $F_{2\alpha}$ ($PGF_{2\alpha}$) levels; nuclear translocation of NF-κBp65; and the expression of COX-2, phospho-NF-κBp65. NF-κBp65, NLRP3, apoptosis-associated speck-like protein (ASC), pro-cysteine aspartate-specific protease 1 (pro-caspase-1), cysteine aspartate-specific protease 1 (caspase-1), interleukin (IL)-1β, and IL-18.

Results: The treatment groups showed considerably reduced pathological uterine injury compared with that of the control. This was associated with decreased $PGF_{2\alpha}$ and increased PGE_2 levels. The uterine tissues in the treatment groups showed reduced NF-κBp65 nuclear translocation and a decreasing trend in COX-2, NF-κBp65, phospho-NF-κBp65, NLRP3, ASC, pro-caspase-1, caspase-1, IL-1β, and IL-18 protein expression compared with that of the controls. The levels of each protein in the parecoxib and ibuprofen groups did not differ considerably from those in the EA group. Furthermore, EA markedly improved pain symptoms and pathological damage in PDM rats and downregulated the expression of COX-2/NF-κB/NLRP3 signaling pathway proteins in uterine tissue.

Conclusion: Our findings demonstrated superior anti-inflammatory effects of EA + parecoxib on COX-2/NF-κB/NLRP3 signaling pathway-related proteins compared with that of EA alone or single-drug administration.

Keywords: anti-inflammatory treatment, cyclooxygenase-2, prostaglandin, nuclear transcription factor, nucleotide-binding oligomerization domain-like receptor 3

Introduction

Primary dysmenorrhea (PDM) refers to the pain prior to or during menstruation without pelvic pathology and is characterized by spastic suprapubic pain.[1,2] PDM affects 50-90% of women worldwide, of which > 50% experience moderate-to-severe pain.[3] PDM is associated with mood disorders and physical discomfort,[4–6] which remarkably reduces the quality of life of affected women;[7] however, the exact underlying mechanisms of PDM remain unclear.

Received: 23 December 2024
Accepted: 8 July 2025
Published: 15 July 2025

PDM is induced by elevated prostaglandin (PG) levels in the uterine tissue.[8] $PGF_{2\alpha}$ stimulates excessive smooth muscle contraction in the uterus, reduces uterine blood flow, induces uterine ischemia and hypoxia, and increases the accumulation of arachidonic acid metabolites, leading to pain.[9] Cyclooxygenase-2 (COX-2) catalyzes the conversion of arachidonic acid into PG.[10]

Nuclear factor κB (NF-κB) proteins bind to the κB sites at the promoters of various genes and regulate the transcription of inflammation-associated genes.[11] When stimulated by external signals, inhibitor of NF-κB (IκB) is phosphorylated by the IκB complex. This enables NF-κB dimers to enter the nucleus from the cytoplasm and activate target genes, thus further aggravating inflammation. Concurrent activation of the NLRP3 inflammasome aggravates the degree of inflammatory infiltration in endometritis and pelvic inflammatory diseases. NF-κB induces the expression of various cytokine genes, including interleukin (IL)-1, IL-6, and IL-8.[12] This activates the NLRP3 inflammasome, ultimately upregulates precursor NLRP3, IL-1β, and IL-18 levels in uterine tissues, and further exacerbates NLRP3 inflammasome activation.[13] Furthermore, IL-1 β and IL-18 induce pain signals.[14,15] Therefore, in PDM, NLRP3 inflammasome activation may be linked to the activation and transcription of NF-κB.[16] Experimental evidence shows that inhibiting NLRP3 inflammasome activity markedly mitigates endometritis.[17,18] COX-2 positively regulates and activates the NLRP3 inflammasome and mitigates inflammatory diseases.[19–21] For example, COX-2 inhibitors reduce NLRP3, caspase-1, and IL-18 expression in epileptic hippocampal tissues[22] and alleviate acute lung injury by suppressing the NLRP3 inflammasome.[23] Collectively, the COX-2/NF-κB/NLRP 3 inflammatory pathway affects the synthesis and release of inflammatory factors; therefore, the pathway is an important mechanism in the development of PDM (Figure 1).

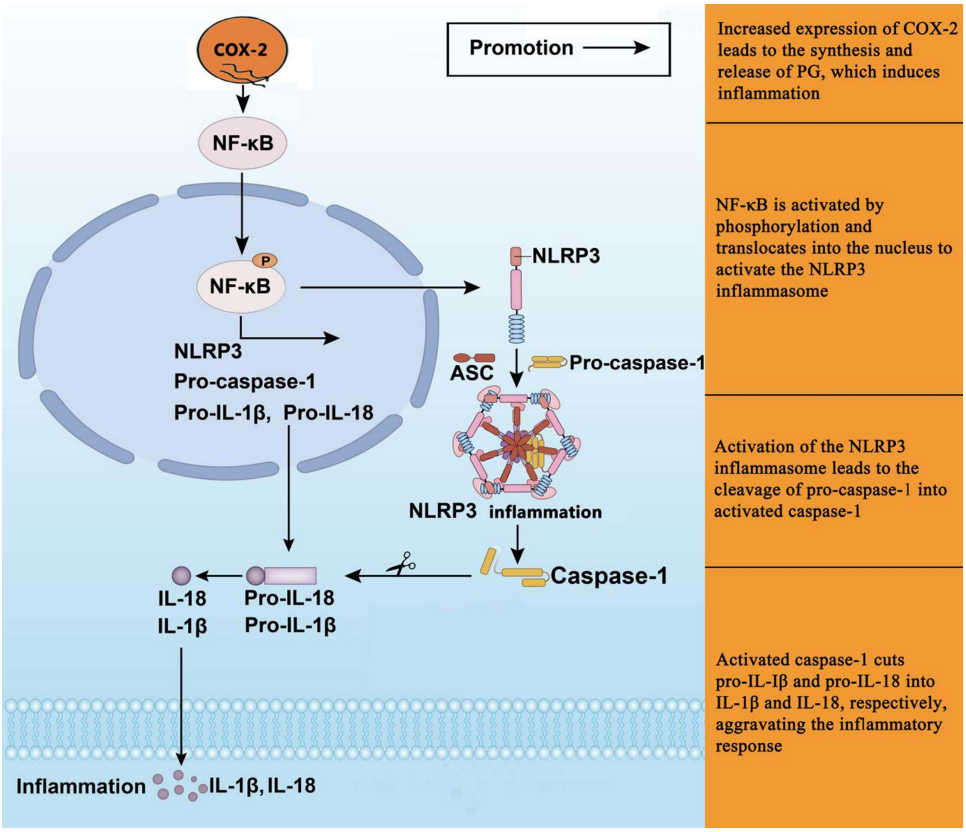

Figure 1 Schematic representation of the COX-2/NF-κB/NLRP3 inflammatory pathway.
Abbreviations: COX-2, cyclooxygenase-2; NF-κB, nuclear factor κB; p-NF-κB, phospho-nuclear factor κB; NLRP3, nucleotide-binding-oligomerization domain-like receptor protein 3; ASC, apoptosis-associated speck-like protein; pro-caspase-1, pro-cysteine aspartic acid-specific protease 1; caspase-1, cysteine aspartic acid-specific protease 1; IL-1β, interleukin-1β; IL-18, interleukin-18.

Electroacupuncture (EA) is an alternative treatment for pain relief that combines acupuncture with electrical stimulation. Compared with oral administration and injection of drugs, EA is safer with fewer side effects and has recently attracted considerable attention. EA has been used to mitigate PDM;[24] however, limited data are available regarding the mechanisms of EA intervention in PDM.

Using a rat model of PDM, we have previously reported that the levels of NLRP3 inflammasome and IL-1β protein in uterine tissue markedly increased, along with inflammatory responses, such as endometrial peeling and edema. We also showed that EA considerably reduced the protein levels of NLRP 3 and IL-1β and inflammation and that the NLRP3-specific inhibitor MCC950 alleviated the release of inflammatory factors by inhibiting NF-κB signaling, suggesting the involvement of NLRP3 in PDM. Studies have revealed that EA exerts an anti-inflammatory effect.[25,26] However, the mechanism of electrical inhibition against the NLRP 3 inflammasome remains unclear.[27,28]

Therefore, in this study, we established a rat model of PDM and analyzed the protein levels of PGs, COX-2, NF-κB, NLRP3, and downstream inflammatory factors to determine the potential mechanisms underlying the effects of EA and the COX-2 inhibitor parecoxib on PDM-associated inflammation. The findings of this study will help reduce the use of non-steroidal anti-inflammatory drugs (NSAIDs) and circumvent the side effects associated with these drugs while relieving menstrual pain.

Materials and Methods

Chemicals and Reagents

The following reagents were purchased from Selleck Chemicals (Houston, TX, USA): estradiol benzoate (No: S411001, $C_{25}H_{28}O_3$, Molecular weight: 376.49), oxytocin (No. P1029, $C_{45}H_{70}N_{12}O_{14}S_2$, molecular weight: 1067.2), and parecoxib (No. S541801, $C_{19}H_{17}N_2NaO_4S$, molecular weight: 392.4). The remaining reagents used were as follows: ibuprofen sustained-release tablets (No: H10900089, specification: 300 mg/tablet, China Tianjin Shike Pharmaceutical Co., Tianjin, China); 0.9% sodium chloride solution (No: H20023250, Shandong Qidu Pharmaceutical Co., Shandong, China); Methylland (No: C12086108, Shanghai MacLean Biochemical Technology Co., Shanghai, China); potassium hydroxide (No:20200929, Sinopharm Group Chemical Reagents Co., Ltd., Shanghai, China); electron mirror fixative fluid (No: G1102, Wuhan Google Biology, Wuhan, China); and 812 embedding agent (No: 90529–77-4, SPI, West Chester, PA, USA).

Rat prostaglandin E_2 (PGE_2) enzyme-linked immunosorbent assay ELISA kit (No: 20211111-J2944) and rat prostaglandin $F_{2\alpha}$ (prostaglandin $F_{2\alpha}$, $PGF_{2\alpha}$) ELISA kit (No: 20211111-J3106) were purchased from Hunan Aifang Biotechnology Co. Ltd. (China). A Hematoxylin and eosin (HE) staining kit (No: C0105) was purchased from Servicebio (Wuhan, China).

The following items were purchased from Servicebio, China: radioimmunoprecipitation assay lysate (No: G2002); bicinchoninic acid (BCA) protein quantification kit (No: G2026); phosphoprotease inhibitors (No: G2007); anti-beta (No: GB15001, 1:2000, Mouse); caspase-1 antibody (No: GB11383, 1:3000, Rabbit); phosphorylated-NF-κB-p65 antibody (No: GB11142-1, 1:3000, Rabbit); NF-κB-p65 antibody (No: GB12142, 1:2000, Mouse). The following antibodies were used: NLRP3 antibody (No: DF7438, Affinity, 1:3000, Rabbit); ASC (No: GB113966, BIOSS, 1:3000, Rabbit); COX-2 antibodies (No: 12282, CST, 1:3000, Rabbit); and pro-caspase-1 (No: GB11383, CST, 1:3000, Rabbit).

Animals

Healthy adult, virgin, specific pathogen-free 6–8-week-old female Sprague–Dawley rats weighing 180–200 g were purchased from Beijing Huafukang Biotechnology Co., Ltd. (SCXK, Beijing; 2019–0008) and maintained in cages, with 10 animals per cage (n = 60 total), in the Institute of Medical Laboratory Animals, Chinese Academy of Medical Sciences. The temperature and humidity of the animal room were maintained at 20–25 °C and 50%–70%, respectively, with 12 h light:12 h dark or 14 h light:10 h dark cycles. The rats were maintained in a natural circadian cycle and fed with standard animal food with *ad libitum* access to water. The bedding was changed twice weekly, and cage disinfection was performed four times per week.

After one week, all 60 rats were randomly assigned to one of the following six groups: Saline, Model, EA, Parecoxib, EA+Parecoxib, and Ibuprofen (positive control). All experimental animal procedures were performed in accordance with the Chinese National Standard Guidelines for Animal Welfare (GB/T35892-2018). This study was conducted in strict accordance with the recommendations of the NIH's Health Guide for the Care and Use of Laboratory Animals. The study protocol was approved by the Institutional Animal Care and Use Committee of Hunan University of Traditional Chinese Medicine (protocol number LL2021040703). All procedures were performed under sodium pentobarbital anesthesia, and efforts were made to minimize distress.

Instruments and Equipment

The following instruments were used in this study: pathological tissue embedding instrument (BM-type, Anhui Research Institute of Electronic Science, Anhui, China); micro camera (Model 20486, Olympus, Tokyo, Japan); direct fluorescence microscope (DM4 B, Leica, Berlin, Germany); high-speed frozen centrifuge (Sorvall ST 16R, Thermo Fisher Scientific, Waltham, MA, USA); electrophoresis apparatus, transmembrane instrument, and gel imaging system (Gel Doc XR, Bio-Rad Laboratories, Hercules, CA, USA); ultrathin slicer EM UC7, Leica, Wetzlar, Germany) and diamond slicing knife (Ultra 45, Diatome AG, Nidau, Switzerland); panoramic slice scanner (3DHISTECH, Budapest, Hungary); ultramicrotomy (HT7700, HITACHI, Tokyo, Japan); electric acupuncture apparatus (SDZ-V type, Suzhou Medical Supplies Factory Co., Ltd., Suzhou, China); AIPathwell automated image analysis software (Servicebio Co, Ltd, Wuhan China).

Development of the PDM Rat Model and Intervention Measures

Except for those in the Saline group, all rats were treated with estradiol benzoate for 10 days and oxytocin intraperitoneally on Day 11 to establish a PDM model. Estradiol benzoate was administered subcutaneously daily at 9 am (dosage on Days 1 and 10: 0.5 mg/rat, Days 2–9: 0.2 mg/rat).[29] Rats in the Saline group were administered an equal volume of 0.9% normal saline instead of the drug. Saline dosages were as follows: Days 1 and 10: 0.5 mL/rat; Days 2–9: 0.2 mL/rat. EA and drug administration were performed in the corresponding treatment groups alongside the treatments used to establish the PDM model. Rats were bound and fixed. For the EA group, the SP 6 and CV 4 acupoints were used.[30] Based on the Acupuncture Point Position of Rats in Experimental Acupuncture and Moxibustion, SP 6 was selected 10 mm above the medial malleolus apex of the hind limb, and CV 4 was selected 25 mm below the umbilicus. The umbilicus is the lower one-fourth and the upper three-quarter intersection between the sternoclavicular joint and pubic symphysis. After routine disinfection of each acupoint, acupuncture was performed using a disposable sterile acupuncture needle (0.30 mm in diameter and 13 mm in length). SP 6 and CV 4 were perpendicularly punctured at 5 and 2 mm, respectively. The positive electrode of the conducting wire was connected to the needle, and the negative electrode was clamped onto the skin next to the acupoint. Electric current was administered as a dense wave at a frequency of 50 Hz[28,31] and a current of 1 mA, with a slight twitch in the local acupoint muscles. An SDZ-V type EA instrument with a pulse width of 0.2 ms ± 30% was used. The treatment was initiated on the first day of modeling and administered once daily for 20 min for 10 consecutive days. Xiao Xue performed all acupuncture procedures. The Parecoxib group was intraperitoneally injected with 10 mg/kg parecoxib sodium solution once daily for 10 days; the EA+Parecoxib group simultaneously received EA and an intraperitoneal injection of 10 mg/kg parecoxib sodium solution once daily for 10 days; the Ibuprofen group was treated with an 0.8 mL intragastric dose (at a concentration of 125 mg/100 mL) of ibuprofen for 10 days. On Day 11 at 9 am, an intraperitoneal oxytocin injection (2 U/rat; concentration: 0.5 mg/mL) was administered to rats in each experimental group, while an equal volume of 0.9% normal saline was administered to the Saline group.

The criterion for successful model establishment in PDM rats was a torsional reaction after oxytocin injection. On Day 11, blood was collected from the abdominal aorta, ELISA was used to assess PGE 2, and PGF2α levels, and HE staining was used to observe the endometrial histopathological morphology of rats. When the PGF2α content is increased, the PGE2 content is decreased, and the tissue observed under HE staining showed histopathological changes, such as increased luminal epithelial necrosis, endometrial edema, and shedding, which indicates that the model is successfully established.

Measurement of the Torsional Response in Rats

We recorded the number of twists and twist latencies in the rats 30 min after oxytocin injection. The criteria for the twist reaction were as follows: development of abdominal depression, trunk and hindlimb extension, and internal rotation of one limb. Twist latency was calculated as the time between oxytocin injection and the first twist reaction[32] while writhing latency was calculated from the intraperitoneal oxytocin injection to the first twist reaction. Twist scores were assigned various levels as follows: level 0 (0 points): normal posture, forepaw flat, or normal exploration behavior; level 1 (1 point): oblique body side; level 2 (2 points): hind limb extension, hind paw dorsiflexion, and body extension with frequent pelvic lateral rotation; level 3 (3 points): abdominal muscle contraction and hind limb posterior extension.[32] Normal exploration and the resulting somatic and hindlimb extensions were not considered twisting.

Blood and Tissue Sample Preparation

After monitoring for behavioral indicators, the rats were anesthetized according to the operating standards of Experimental Zoology, and subsequently weighed and administered an intraperitoneal injection of 0.3 mL/100 g of 2% sodium pentobarbital solution. Blood samples were collected from the abdominal aorta under anesthesia. The uterine tissue was harvested via laparosection, stored on ice discs, and processed to observe the uterine tissue morphology.

HE Staining of Uterine Tissues

A sample of uterine tissue (5-mm sections) from five rats in each group was removed, fixed in 4% paraformaldehyde solution in Eppendorf tubes, and stored at 20–25 °C for approximately 24 h. The fixed rat uterine tissues were dehydrated using an ethanol gradient, treated with xylene for transparency, paraffin-embedded, and machine-sectioned, followed by dewaxing and hydration of paraffin sections. HE staining was performed as follows: the tissues were initially stained with hematoxylin, subjected to differentiation and blue counterstaining with eosin, washed with water, dehydrated, made transparent, and sealed. Histopathological changes in the rats from all groups were observed under a light microscope. Histopathological damage was scored based on degeneration and necrosis of the endometrium and myometrium, inflammatory cell infiltration-induced morphological changes, edema, and increased gland size.[33] Based on the microscopic morphological features of the uterus, the following histopathological scores were assigned as follows: 0, uterine without pathology; 1, endometrial degeneration and necrosis; 2, lamina propria edema; 3, glandular increase in the lamina propria; 4, inflammatory cell infiltration into the lamina propria; 5, myometrial inflammation.

Transmission Electron Microscopy (TEM)

Uterine tissue sections not exceeding 1 mm × 1 mm × 1 mm were obtained, separated using an electron microscope fix fluid, fixed at 4 °C for 2–4 h, and rinsed with 0.1 M phosphate buffer (PB) (pH 7.4) thrice for 15 min and 1% osmium 0.1 M PB (pH 7.4) for 2 h at approximately 20 °C. The tissues were then rinsed with 0.1 M PB (pH = 7.4) thrice for 15 min and successively dehydrated in 50, 70, 80, 90, 95, and 100% alcohol, followed by treatment with 50:50 alcohol–acetone solvent and 100% acetone (15 min) for final dehydration. The tissues were further processed as follows: acetone, 812 embedding agents (1:1) for 2–4 h, acetone, 812 embedding agents (2:1) overnight, and pure 812 embedding agents for 5–8 h performed at room temperature. The samples were incubated with a pure 812 embedding agent in an embedded plate in an oven at 37 °C overnight, and polymerization was performed in an oven at 60 °C for 48 h. After obtaining ultrathin sections (60–80 nm), uranium–lead double staining (2% uranium acetate–saturated alcohol solution and lead citrate, stained for 15 min each) was performed, and the sections were dried at 25 °C overnight. Images were acquired using TEM.

ELISA

Blood samples were collected from the abdominal aorta (5 mL), and the collected blood was allowed to stand for 1–2 h and subsequently centrifuged in a porous centrifuge at 3500 rpm for 10 min. Serum (1–2 mL) from each tube was aliquoted into disposable Eppendorf tubes using a pipette gun and stored in a –20 °C refrigerator for further analysis. Ipsilateral uterine tissue (0.2–1 g) was also used to make a 10% tissue homogenate. The homogenate was centrifuged at a radius of 15 cm at 3000 rpm for 20 min. The supernatant was aliquoted into Eppendorf tubes and stored at –80 °C for

further use. PGE_2 and $PGF_{2\alpha}$ levels were evaluated using ELISA according to the manufacturer's instructions. The PG content was expressed as pg/mL.

Immunofluorescence Detection

A part of the ipsilateral segment of the uterine tissue from each group was obtained, washed, fixed, embedded, sectioned, and incubated with the primary antibody of nuclear transcription factor p65 (NF-κBp65) (1:100) at 4 °C with shaking for 48 h.

After rinsing in phosphate-buffered saline, the sections were incubated with horseradish peroxidase (HRP)-labeled goat anti-mouse secondary antibody at 25 °C with shaking for 1 h. After rinsing, an anti-fluorescence quencher was added to the section, and the glass slides were sealed and stored without light exposure. The AIPathwell automated image analysis software was used for image analysis. AIPathwell, a digital pathology image analysis software based on artificial intelligence (AI) learning launched by Servicebio, uses the principle of AI deep learning to train an algorithm using massive data for automated image analysis. The software automatically localizes the nuclei and extends the cytoplasmic range. AIPathwell uses AI technology to identify blue nuclei in the entire tissue section, counts the total cell number, and then identifies the red fluorescence in the whole tissue section as a positive signal, including a positive signal in the cytoplasmic range or the nucleus. The number of cells with positive nuclei (purple-red color) was counted separately. The nucleation rate was calculated using the following formula:

NF-κBp65 nucleus entry rate = nucleus positive cell count/(nucleus positive cell count + cytoplasm positive cell count).

Western Blotting

Uterine tissue (30 mg) was collected from the same side of the rats in each group. The tissue was ground using a grinding machine at 0–10 °C and lysed on ice in pre-cooled radioimmunoprecipitation assay lysis buffer containing protease and phosphorylase inhibitors for 30 min. The sample was then centrifuged at a radius of 140 mm at 3500 rpm and 4 °C for 10 min. Subsequently, the supernatant containing the total tissue protein was collected, and after the sample buffer was added, the sample was heated in a boiling water bath for 10 min to fully denature the proteins.

A BCA protein assay kit was used to determine the protein concentration based on a standard protein curve, and the protein concentration was balanced within the samples. After electrophoresis, polyvinylidene fluoride membrane transfer, and blocking with TBST, the membranes were incubated overnight at 4 °C with the following specific primary antibodies diluted with Tris-buffered saline Tween-20: COX-2 (1:2000), phosphorylated-NF-κB-p65 (1:3000), NF-κB-p65 (1:2000), NLRP3 (1:1000), ASC (1:3000), caspase-1 (1:3000), pro-caspase-1 (1:3000), IL-1β (1:3000), IL-18 (1:3000), and β-actin (1:2000). The membranes were then washed with Tris-buffered saline containing Tween-20 and incubated with diluted secondary antibodies for 60 min. Finally, membranes were developed using enhanced electroluminescence reagents. The original figures are presented in the Supplementary materials.

Statistical Analyses

Statistical analyses were performed using IBM SPSS Statistics for Windows, version 26.0 (IBM Corp., Armonk, N.Y., USA). Mapping was performed using Prism 8.0 software (GraphPad Software, San Diego, CA, USA). Data visualization was performed using R software (version 4.4.2), and data are expressed as the mean ± standard deviation. If the data satisfied the normality and homogeneity of variance assumptions, a one-way analysis of variance was used, otherwise, the Kruskal–Wallis *H*-test was used. To account for multiple comparisons, statistical significance was adjusted using the Bonferroni correction. Statistical significance was set at $P < 0.05$.

Results

EA Reduced the Writhing Response and Prolonged the Latency of Torsion

To determine whether EA relieved pain in PDM model rats, the effects of electro-targeting on estradiol benzoate- and oxytocin-induced PDM were examined (Supplementary Tables 1–3). At 30 min, expectedly, rats in the Saline group

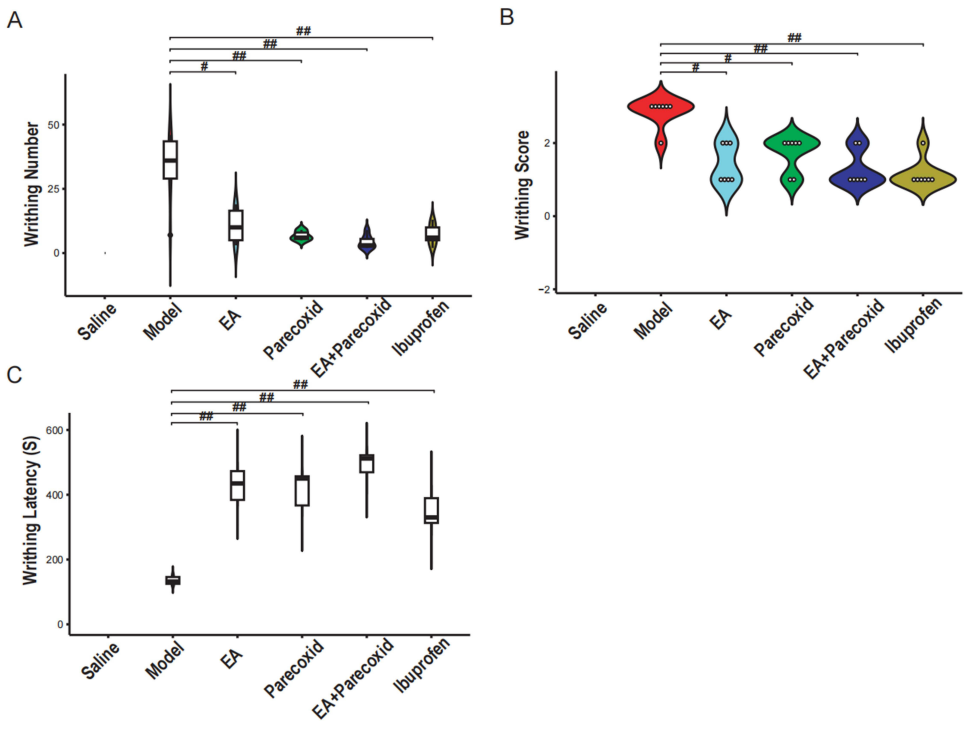

Figure 2 Comparison of writhing number, score, and latency 30 min after oxytocin injection. The writhing behavior of each rat was recorded separately. (**A**) Writhing number is the number of writhing episodes. (**B**) Writhing score is the highest score within 30 min. (**C**) Writhing latency is the time interval from oxytocin injection to the first writhing reaction. Box plots include the median (central line), interquartile range (IQR; box boundaries), and the full data range (whiskers extending to the minimum and maximum values). Dot plots have individual data points for each group, and reveal the distribution, variability, and potential outliers within each category. Dot and box plots have the same underlying individual-level data, with dot plots including each data point and box plots summarizing the distribution. Statistical analyses were conducted using the Kruskal–Wallis *H*-test (n = 10). $^{\#}P < 0.05$ and $^{\#\#}P < 0.01$ compared with the Model group.

showed no torsion response since they were not treated with oxytocin, whereas those in the Model group showed significantly increased writhing numbers, scores, and latency (Figure 2A–C, $P < 0.01$). Compared with the Model group, each treatment group showed significantly decreased writhing numbers and scores (Figure 2A–C, $P < 0.05$, $P < 0.01$) with significantly prolonged writhing latency (Figure 2C, $P < 0.01$). No difference was observed in the writhing response among the EA, Parecoxib, EA+Parecoxib, and Ibuprofen groups (Figure 2C, $P > 0.05$).

EA Alleviated Endometrial Cell Injury and Reduced Pathological Uterine Damage in PDM Model Rats

Tissue sections of the uterus were stained with HE and observed under a light microscope to evaluate the protective effect of EA on endometrial cell injury. The Saline group showed intact mucosal epithelium, with no significant epithelial cell degeneration and necrosis or neutrophil infiltration in the endometrium.

Compared with the Saline group, the Model group displayed more luminal epithelial necrosis and severe endometrial edema accompanied by extensive shedding. The nucleus was initially firm, but eventually fragmented and disappeared. The endometrium was associated with neutrophil infiltration and the gland cavity was mildly dilated. The EA group showed high luminal epithelial necrosis and mild endometrial edema. The Parecoxib group showed necrosis of the individual luminal epithelium; the nucleus was initially firm, but eventually fragmented and disappeared, with minimal neutrophil infiltration into the endometrium. The EA+Parecoxib group showed minimal luminal epithelial necrosis. The nucleus was initially firm, but eventually fragmented and disappeared; hence, no significant inflammatory cell infiltration was observed in the endometrium. Similarly, no significant inflammatory cell infiltration was observed in the endometrium of the ibuprofen-treated group (Figure 3A). HE pathology lesion scores were significantly higher in the Model than those in the Saline groups (Figure 3B, $P < 0.01$). However, the EA (Figure 3B, $P < 0.05$), Parecoxib, EA+Parecoxib, and Ibuprofen (Figure 3B, $P < 0.01$) groups showed significantly lower HE pathology lesion scores than the Model group.

https://doi.org/10.2147/JPR.S512243

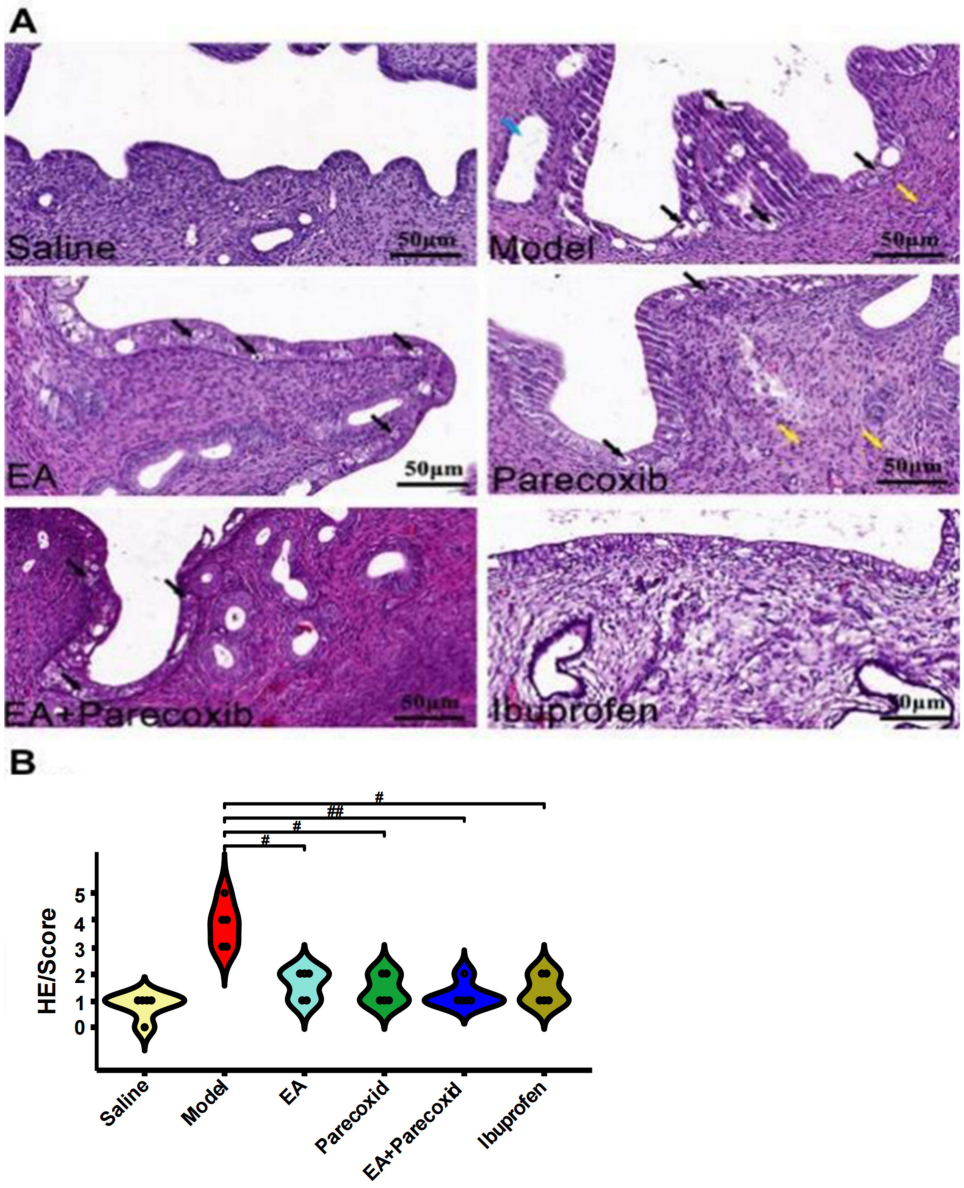

Figure 3 Comparison of histopathological changes and uterine morphology among study groups. (**A**) Pathological damage in each group was determined using HE staining. Blue, black, and yellow arrows indicate mild expansion of the gland cavity, luminal epithelial necrosis, hyperemia, and neutrophil infiltration, respectively. (**B**) Pathological scoring: histopathological scoring of uterine microstructural features in each group. Dot plots have individual data points per group, and reveal the distribution, variability, and potential outliers within each category. Statistical analyses were performed using the Kruskal–Wallis *H*-test (n = 5). $^{\#}P < 0.05$ and $^{\#\#}P < 0.01$ compared with the Model group.

Abbreviation: HE, hematoxylin and eosin.

The HE pathology scores were not significantly different between the EA, Parecoxib, EA+Parecoxib, and Ibuprofen groups (Figure 3B, $P > 0.05$) (Supplementary Table 4).

Morphological Changes in Each Group Analyzed Using TEM

In the Saline group, endometrial fibroblasts showed regular shape with no evident cytoplasm edema, less mitochondrial membrane damage, and no gross endoplasmic reticulum (RER) or significant degranulation. In the Model group, endometrial fibroblasts showed irregular shape, evident cytoplasmic edema, oval mitochondria, severe swelling, slight expansion of superficial endoplasmic reticulum (ER), and significant degranulation. In the drug/EA groups, the endometrial fibroblasts were spindle-shaped, with oval mitochondria, uniform matrix, slightly higher electron density, small

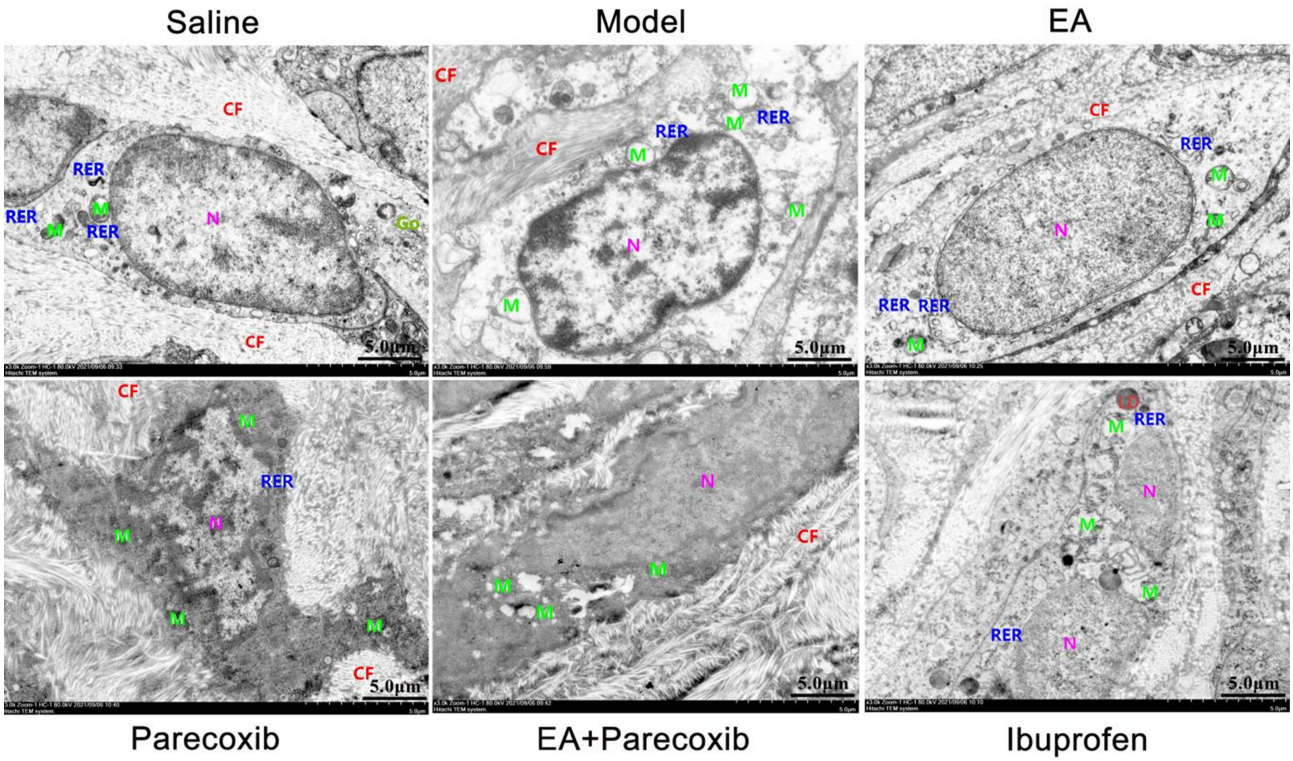

Figure 4 Transmission electron microscopy images of uterine tissue from each group. Histopathological changes in the morphology and ultrastructure of the rat uterine tissue in all six groups were observed using transmission electron microscopy.
Abbreviations: CF, collagen fibers; N, nucleus; M, mitochondria; RER, rough endoplasmic reticulum; Go, Golgi; LD, lipid droplets.

and shortened fracture, and smaller mitochondria. The ER showed moderate expansion and retention and very little degranulation. This indicates that electroacupuncture can reduce endometrial fibroblast cytoplasmic edema and mitochondrial membrane damage (Figure 4).

EA Downregulated PGF2α and Increased PGE2 Levels in Serum and Uterine Tissue of PDM Model Rats

PGs are involved in PDM pathogenesis, and clinical trials have revealed that $PGF_{2\alpha}$ inhibitors effectively improve PDM.[34] Therefore, PGs can be used to evaluate whether the design of a PDM animal model was successfully established. The serum and uterine $PGF_{2\alpha}$ levels were significantly higher, while PGE_2 levels were significantly lower in the Model group (Figure 5, $P < 0.01$) than those in the Saline group. $PGF_{2\alpha}$ levels were decreased, whereas PGE_2 levels were increased in the EA, Parecoxib, EA+Parecoxib, and Ibuprofen groups compared with those in the Model group (Figure 5, $P < 0.01$). However, these levels were not significantly different among the EA, Parecoxib, EA+Parecoxib, and Ibuprofen groups (Figure 5, $P > 0.05$) (Supplementary Tables 5–8).

EA Downregulated COX-2 Protein Levels in the Uterine Tissue of PDM Model Rats

We observed the effect of EA on the expression of COX-2, which is an upstream regulator of PG. As expected, uterine COX-2 protein levels in the Saline group were very low and undetectable by immunoblotting; however, these levels were significantly higher in the Model group (Figure 6, $P < 0.01$). COX-2 protein levels in the EA, Parecoxib, EA+Parecoxib, and Ibuprofen groups were significantly lower than those in the Model group (Figure 6; $P < 0.01$). Compared with those in the EA+Parecoxib group, COX-2 protein levels were significantly increased in the EA and Parecoxib groups (Figure 6, $P < 0.01$). Compared with the Ibuprofen group, COX-2 protein levels in the EA+Parecoxib group were significantly lower (Figure 6, $P < 0.01$); however, no significant difference in COX-2 levels was detected among the EA, Parecoxib, and Ibuprofen groups (Figure 6, $P > 0.05$) (Supplementary Figures 1–6).

https://doi.org/10.2147/JPR.S512243

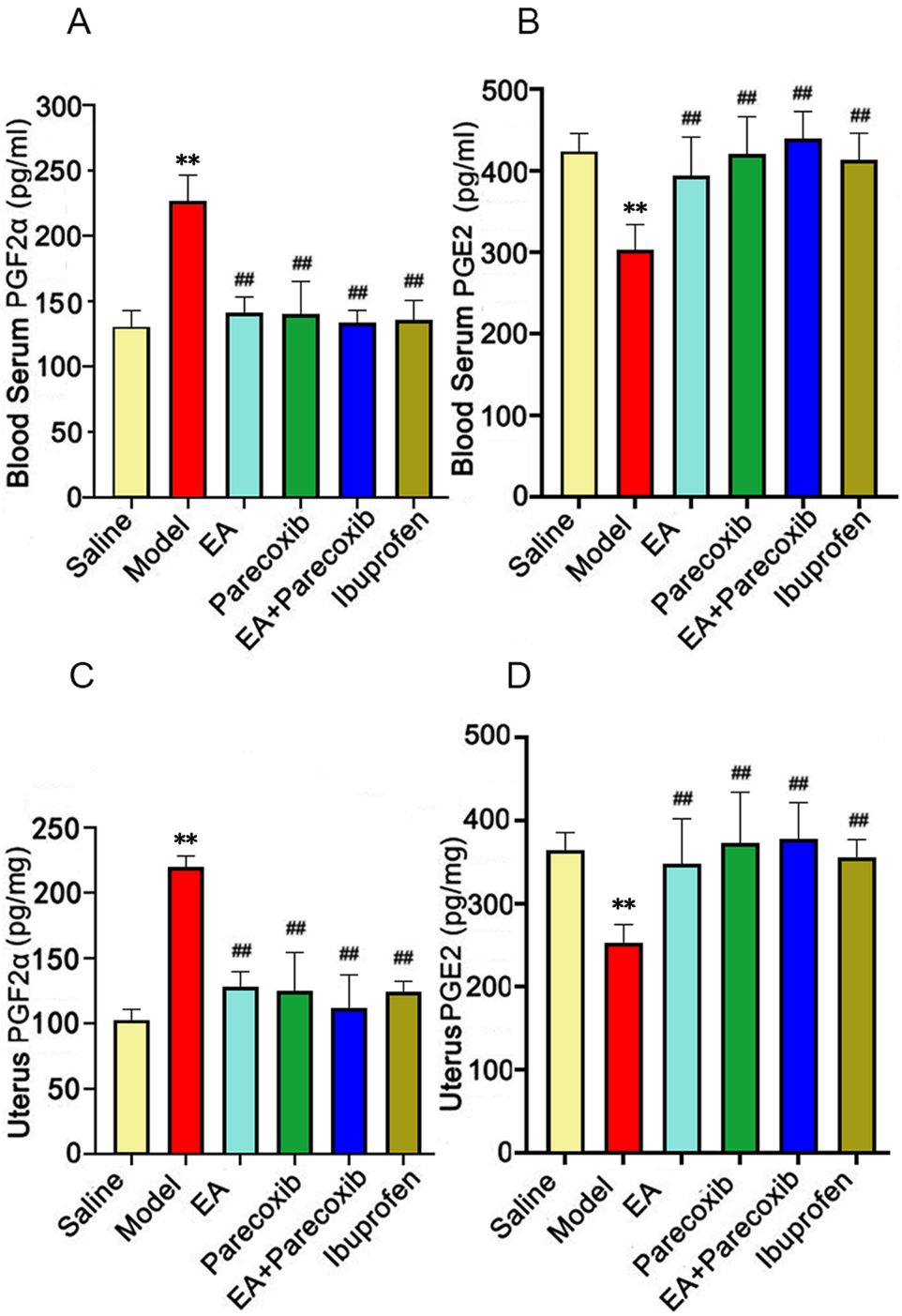

Figure 5 Comparison of serum and uterine $PGF_{2\alpha}$ and PGE_2 levels among different groups. An enzyme-linked immunosorbent assay (ELISA) was employed to determine $PGF_{2\alpha}$ and PGE_2 levels in the serum and uterus. (**A**) Blood serum PGF2α levels in each group. (**B**) Blood serum PGE2 levels in each group. (**C**) Uterus PGF2α levels in each group. (**D**) Uterus PGE2 levels in each group. Data are means ± SD (n = 10). $^{**}P < 0.01$ compared with the Saline group and $^{\#\#}P < 0.01$ compared with the Model group. **Abbreviations**: $PGF_{2\alpha}$, prostaglandin $F_{2\alpha}$; PGE, prostaglandin E_2; SD, standard deviation.

EA Inhibited NF-κBp65 Nuclear Translocation in Rat Uterine Tissues

To determine whether EA is directly involved in NF-κBp65 inhibition by COX-2, we investigated NF-κB nuclear translocation using immunofluorescence. The uterine epithelial cytoplasm of the Saline group was weakly positive, whereas that of the Model group was strongly positive with several positive nuclei. The other treatment groups were positive for uterine epithelial cytoplasm, with fewer positive nuclei than the Model group. The number of NF-κBp65-

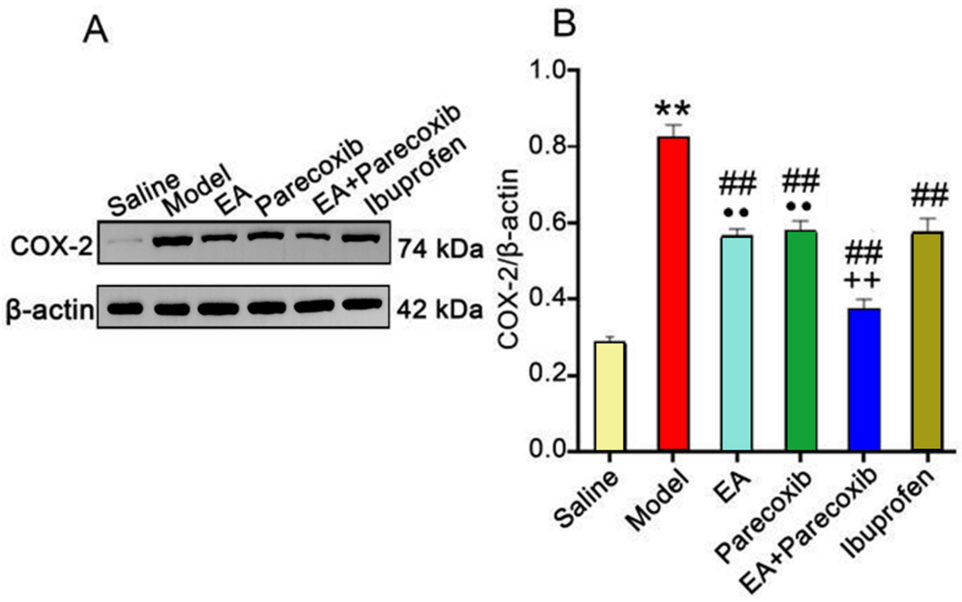

Figure 6 Comparative analysis of uterine COX-2 protein expression in rats from different groups. Western blot analysis was utilized to quantify COX-2 expression in rats of each group, with β-actin serving as a control. No upregulation of COX-2 expression was observed among rats in the Saline group. The molecular weight of COX-2 is 74 kDa, and that of β-actin is 42 kDa. (**A**) Western blot images of COX-2 and β-actin proteins in different groups. (**B**) Bar chart of the relative expression of COX-2 normalized to that of β-actin. Data are presented as means ± SD (n = 5). Compared with the Saline group, $^{**}P < 0.01$; compared with the Model group, $^{\#\#}P < 0.01$; compared with the EA+Parecoxib group, $^{\bullet\bullet}P < 0.01$; compared with the Ibuprofen group, $^{++}P < 0.01$.
Abbreviations: COX-2, cyclooxygenase-2; SD, standard deviation.

positive cells was higher in the Model than Saline groups (Figure 7, $P < 0.01$) and significantly reduced in the other treatment groups (Figure 7, $P < 0.01$). The number of cells positive for NF-κBp65 translocation was significantly reduced in the EA+Parecoxib group compared with that in the Ibuprofen group (Figure 7, $P < 0.01$). However, the rate of NF-κBp65 translocation into nuclear-positive cells was not significantly different among the EA, Parecoxib, and Ibuprofen groups (Figure 7, $P > 0.05$) (Supplementary Table 9).

EA Inhibited NF-κBp65 Activation in the Uterine Tissue of PDM Model Rats

To confirm whether the decrease in phospho-NF-κBp65 and NF-κBp65 was caused by the impairment of the COX-2 activation signal, we investigated NF-κBp65 expression using immunoblotting.

As expected, the uterine phospho-NF-κBp65 and NF-κBp65 levels in the Saline group were extremely low and undetectable by immunoblotting; however, these levels were significantly elevated in the Model group (Figure 8, $P < 0.01$). Furthermore, these levels were significantly reduced in the EA, EA+Parecoxib, and Ibuprofen groups compared with those in the Model group (Figure 8, $P < 0.01$), and significantly lower in the EA+Parecoxib group compared with those in the Ibuprofen group (Figure 8, $P < 0.01$).

Compared with the EA+Parecoxib group, these levels were significantly increased in the EA group and the parecoxib group (Figure 8, $P < 0.01$). However, no significant differences were observed among the EA, Parecoxib, and Ibuprofen groups (Figure 8, $P > 0.05$) (Supplementary Figures 1–6).

EA Inhibited NLRP3 Inflammasome Activation and Reduced the Levels of its Downstream Inflammatory Factors IL-1β and IL-18

We examined the expression of NLRP3, pro-caspase-1, ASC, caspase-1, and IL-1β, IL-18 levels in uterine tissues using immunoblotting to determine whether COX-2 regulated NF-κB-mediated activation of the NLRP3 inflammasome. Western blotting revealed low levels of NLRP3, pro-caspase-1, ASC, caspase-1, and IL-1β, IL-18 in the uterine tissues of the saline-injected mice.

https://doi.org/10.2147/JPR.S512243

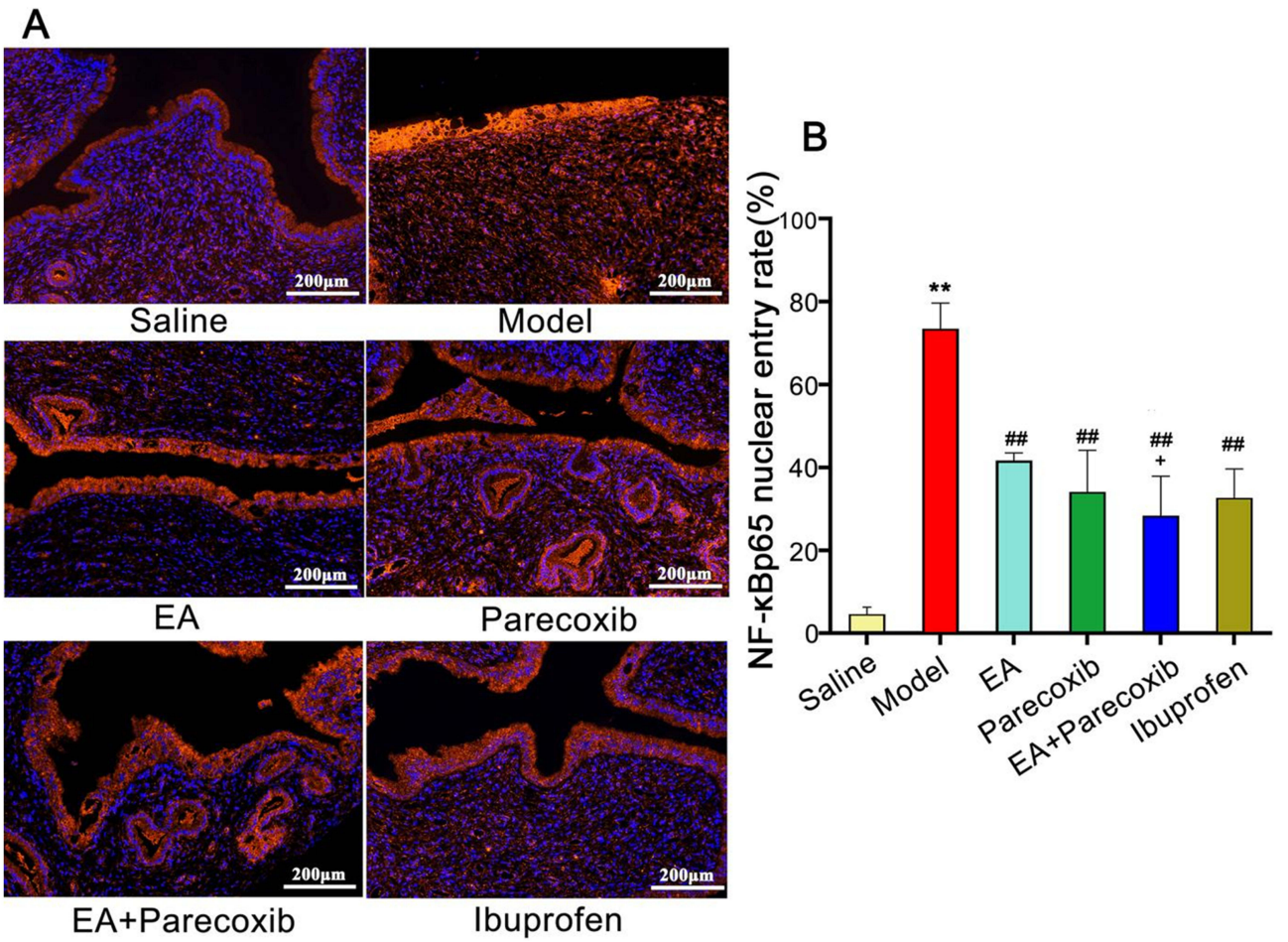

Figure 7 Immunofluorescence analysis of NF-κBp65 expression in rat uterine tissues. Fluorescence analysis software (AIPathwell), which uses AI technology, was used to identify localized cells (blue nuclei) in whole tissue sections to count the total cell number. The AI software identified red fluorescence in the whole tissue section as a positive signal for NF-κBp65 expression. When NF-κBp65 was expressed only in the cytoplasm, a red fluorescence signal was detected around the blue nucleus. When NF-κBp65 is also expressed in the nucleus, the red fluorescent signal in the nucleus overlaps with the blue fluorescence, leading to a purplish-red fluorescent signal. NF-κBp65 nuclear entry rate = nucleus positive cell count/(nucleus positive cell count + cytoplasm positive cell count). (**A**) Immunofluorescence images of NF-κBp65 expression in different groups; scale bar = 200 μm. (**B**) Bar chart of the NF-κBp65 nuclear entry rate (%) for each group. Data are means ± SD (n = 3).$^{**}P < 0.01$, compared with the Saline group; $^{\#\#}P < 0.01$, compared with the Model group; $^{+}P < 0.05$, compared with the Ibuprofen group.
Abbreviations: NF-κB, nuclear factor κB; AI, artificial intelligence; EA, electroacupuncture.

The Model group showed that the protein levels of these downstream inflammatory factors were significantly increased compared with those in the Saline group (Figure 9, P < 0.01). However, compared with the Model group, the protein levels of NLRP3, pro-caspase-1, caspase-1, IL-1β, and IL-18 were significantly decreased in the EA group (Figure 9, P <0.05, P <0.01), but the differences in ASC levels were not significant (Figure 9, P >0.05); compared with the Model group, the protein levels of NLRP3, pro-caspase-1, ASC, caspase-1, IL-1β, and IL-18 were significantly decreased in the Parecoxib (Figure 9, P <0.05, P <0.01), EA+Parecoxib (Figure 9, P <0.01), and Ibuprofen groups (Figure 9, P <0.05, P <0.01).

Compared with the EA+Parecoxib group, the levels of NLRP3, pro-caspase-1, IL-1β, and IL-18 were significantly increased in the EA group (Figure 9, P < 0.05, P < 0.01). ASC and caspase-1 levels were not significantly different (Figure 9, P > 0.05). Compared with those in the EA+Parecoxib group, the protein levels of NLRP 3, pro-caspase-1, IL-1β, and IL-18 were significantly higher in the Parecoxib group (Figure 9, P < 0.01), however, the caspase-1 and ASC levels were not significantly different (Figure 9, P > 0.05). Compared with the Ibuprofen group, the EA+Parecoxib group showed a significant decrease in the protein levels of ASC and caspase-1 (Figure 9, P < 0.05), NLRP3, pro-caspase-1, IL-1β, and IL-18 (Figure 9, P <0.01). Moreover, compared with the Ibuprofen group, these protein levels in the EA and Parecoxib groups were not significantly different (Figure 9, P > 0.05) (Supplementary Figures 1–6).

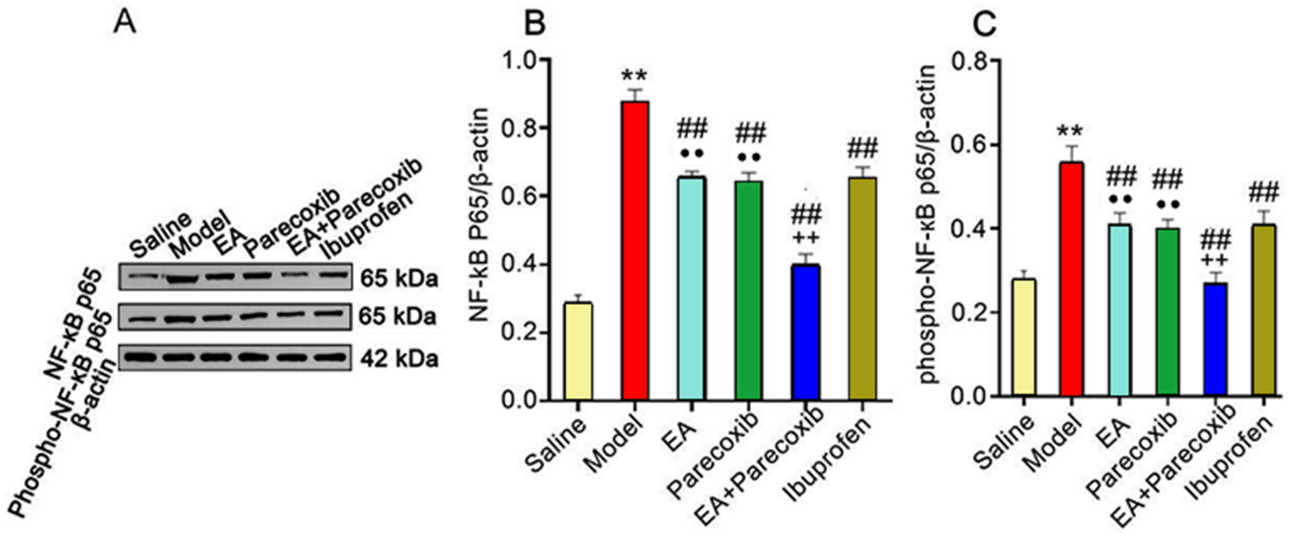

Figure 8 Comparative analysis of phospho-NF-κBp65 and NF-κBp65 protein expression in different groups. Western blot analysis was used to determine the expression of phospho-NF-κBp65 and NF-κBp65 in each group. (**A**) Western blot images of phospho-NF-κBp65, NF-κBp65, and β-actin protein expression in different groups. The molecular weight of phospho-NF-κB p65 and NF-κB p65 is 65 kDa, and that of β-actin is 42 kDa. (**B**) Bar chart of relative NF-κB p65 expression normalized to β-actin for each group. (**C**) Bar chart of the relative phospho-NF-κB p65 expression levels normalized to β-actin for each group. Data are the means ± SD (n = 5). $^{**}P < 0.01$ compared with the Saline group, $^{\#\#}P < 0.01$ compared with the Model group, $^{\bullet\bullet}P < 0.01$ compared with the EA + parecoxib group, and $^{++}P < 0.01$ compared with the Ibuprofen group. Abbreviations: NF-κB, nuclear factor κB; SD, standard deviation; EA, electroacupuncture.

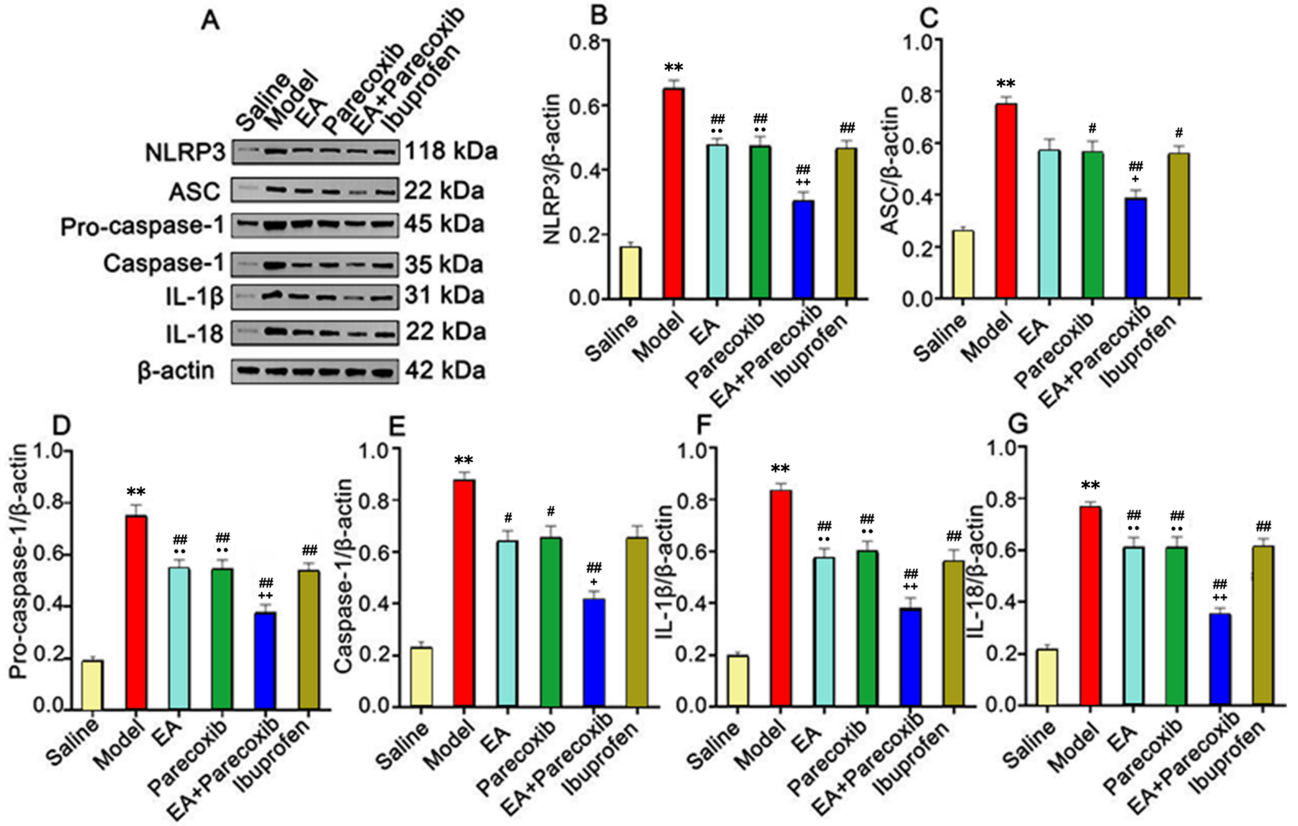

Figure 9 Western blot analysis of NLRP3, pro-caspase-1, ASC, caspase-1, IL-1, and IL-18 protein expression levels. NLRP3, pro-caspase-1, ASC, caspase-1, IL-1, and IL-18 protein expression was analyzed in rat uterine tissues of all groups using Western blotting. (**A**) Western blot images of NLRP3 (118 kDa), ASC (22 kDa), Pro - caspase - 1 (45 kDa), Caspase - 1 (35 kDa), IL - 1β (31 kDa), IL - 18 (22 kDa), and β - actin (42 kDa)protein expression in different groups. (**B**–**G**) Relative expression of (**B**) NLRP3 (**C**) ASC, (**D**) pro-caspase-1, (**E**) caspase-1, (**F**) IL-1β, and (**G**) IL-18 in each group normalized to β-actin. Data are the means ± SD (n = 5). $^{**}P < 0.01$ compared with the Saline group, $^{\#\#}P < 0.01$ compared with the Model group, $^{\bullet\bullet}P < 0.01$ compared with the EA + parecoxib group, and $^{++}P < 0.01$ and $^{+}P < 0.05$ compared with the Ibuprofen group. **Abbreviations**: NLRP3, nucleotide-binding oligomerization domain-like receptor protein 3; ASC, apoptosis-associated spec-like protein; IL, interleukin; SD, standard deviation.

https://doi.org/10.2147/JPR.S512243

Discussion

In this study, we aimed to explore the effects of EA and parecoxib on inflammatory injury in a PDM rat model. A particular focus was placed on the potential involvement of the COX-2/NF-κB/NLRP3 signaling pathway. Our findings suggest that both EA and parecoxib considerably reduce inflammatory injury, as evidenced by improved behavioral and histopathological outcomes.

Estradiol benzoate and oxytocin were used to establish the PDM rat model.[35] Estrogen increases uterine sensitivity by regulating cell proliferation and angiogenesis[16] and by increasing oxytocin receptor (OTR) mRNA expression.[36] Oxytocin induces uterine contractions,[37] thereby causing relative ischemia and hypoxia, which leads to pain. When activated by estrogen, OTRs are overexpressed, and their levels determine the endometrial sensitivity to oxytocin stimulation.[38,39] The spastic contraction of the uterine smooth muscle induced by oxytocin combined with estradiol benzoate is a recognized pathological model of dysmenorrhea-like reactions.

PG influences the inflammatory response in PDM, and the mechanism of dysmenorrhea is associated with increased PGF2α and decreased PGE2 levels in the uterine tissue.[9] Furthermore, increased PGF2α levels are the primary contributor to menstrual pain.[40,41] Compared with those in the Saline group, $PGF_{2\alpha}$ levels in the Model group increased considerably, whereas PGE2 levels decreased. However, the EA group exhibited the opposite effect, thus implying that EA inhibits the elevation of PG levels. EA efficacy was comparable with that of parecoxib sodium or ibuprofen, thereby suggesting that EA can treat PDM by regulating PG levels.

Our results showed that compared with that in the Saline group, the writhing number and scores were increased, torsion latency was markedly shortened, remarkable inflammatory damage occurred in the endometrium, and serum $PGF_{2\alpha}$ and PGE2 levels were increased in the model group, which confirms successful model establishment. An ideal NSAID selectively inhibits PG synthesis. Therefore, an inducible type of COX-2 may ameliorate PDM. Parecoxib sodium, a COX-2 inhibitor, exerts anti-inflammatory and analgesic effects by specifically inhibiting arachidonic acid synthesis via PGs.[42] Parecoxib sodium extensively inhibits the excessive stress response and reduces the level of inflammatory factors.[43] Moreover, the drug produces fewer adverse effects on the gastrointestinal tract than those produced conventional NSAIDs.[44,45] Currently, parecoxib sodium is used for postoperative analgesia to relieve neuropathic pain.[46–48] Parecoxib sodium inhibits spontaneous and PG-induced uterine smooth muscle contraction in rats, thus suggesting its potential in PDM treatment.[49] However, further research exploring the application of parecoxib sodium to block inflammatory injury in PDM and alternative anti-inflammatory therapies and low-toxicity treatment modalities for PDM is required.

NSAIDs are the first-line treatment for PDM.[3] Ibuprofen, a PG synthase inhibitor predominantly used for treating dysmenorrhea, inhibits COX-1, COX-2, and $PGF_{2\alpha}$ synthesis.[50–53] However, ibuprofen may have severe gastrointestinal effects and impair renal function,[54,55] thus limiting its clinical application. In this study, ibuprofen was used as a positive control because of its documented efficacy in dysmenorrhea treatment.

We tested the effects of EA, parecoxib sodium, EA + parecoxib, and ibuprofen intervention on the levels of COX-2 protein, an upstream regulator of PG, in PDM rats. As expected, the COX-2 protein levels in the uterine tissues of the Saline group were very low and could therefore not be detected using immunoblotting. However, COX-2 was markedly increased in the uterine tissue of the Model group, thus confirming uterine histopathological changes in the experimental animals. This suggests that the abundance of COX-2 is very low under physiological conditions but elevated upon inflammatory stimulation. The effective increase of COX-2 protein levels in PDM rats was reversed in each treatment group. In this study, the EA + Parecoxib group showed the greatest reduction in COX-2 levels in uterine tissue and pathological inflammatory responses. Therefore, we conclude that EA and intraperitoneal injection of parecoxib effectively binds COX-2 and exerts an inhibitory effect.

One of the key findings of our study is the potential involvement of the COX-2/NF-κB/NLRP3 signaling pathway in mediating the anti-inflammatory effects of EA and parecoxib. The suppression of this pathway may play a critical role in reducing the inflammatory injury observed in the PDM rat model. To verify that the decreased phospho-NF-κB p65 and NF-κB p65 is caused by impaired COX-2 activation, we used immunofluorescence to investigate the nuclear translocation of NF-κBp65. Immunofluorescence and immunoblotting revealed a markedly high rate of NF-κB p65 nuclear

translocation and increased phospho-NF-κBp65 and NF-κBp65 protein expression in the Model group. This indicated altered histopathology and increased expression of inflammatory factors in uterine tissue. After EA and drug administration, the levels of NF-κB p65 nuclear-positive cells, phospho-NF-κB p65, and NF-κB p65 were considerably reduced, whereas NF-κB expression was reversed; hence, these treatments decreased NF-κB signaling.

NLRP3 inflammasome activation occurs following post-translational modification of NLRP3 inflammasome components (including NLRP3, ASC, and pro-caspase-1), followed by NLRP3 activation and NLRP3 inflammasome formation.[56] As a nuclear transcription factor, NF-κB upregulates the expression of proinflammatory factors, such as the NLRP3 inflammasome and its downstream cytokines (IL-1β and IL-18), after entering the nucleus in uterine tissue. NLRP3 inflammasome activation aggravates the symptoms of endometritis and pelvic inflammatory diseases, such as the degree of inflammatory infiltration in gynecological conditions. The NLRP3 inflammasome is also a regulator of the secretion of proinflammatory factors.[19] The inflammatory response in PDM is primarily mediated by proinflammatory factors, including IL-1, IL-1β, and tumor necrosis factor-α.[57] The NLRP3 inflammasome is involved in several gynecological conditions, such as cervical cancer, preterm birth, postnatal inflammation, mycoplasma infections, and chlamydial infections.[58,59]

EA ameliorates NLRP3 inflammasome activation in the brain.[60,61] Mokhtari et al[62] found that exogenous melatonin alleviated affective disorders caused by neuropathic pain by inhibiting the NF-κB/NLRP 3 pathway and cell apoptosis. Tang et al[35] observed that the NLRP3 inflammasome is activated and expressed in PDM, and MCC950 improves PDM by reducing IL-1β and IL-18 levels by inhibiting the NLRP3 inflammasome. Using a mouse model of postoperative cognitive dysfunction, Sun et al[63] found that EA induced NF-κB signal inhibition and NLRP3 inflammasome activation, thus improving neuroinflammation-related postoperative cognitive dysfunction. Additionally, in a mouse model of diabetic nephropathy, EA intervention inhibited NLRP3 inflammasome activation, thereby protecting against diabetic nephropathy-induced inflammation.[64] We previously reported that EA reduced the protein expression of NF-κB and NLRP3 inflammasome in the uterine tissue of PDM rats.[28] The results of that study confirmed that all treatments inhibited the activation of the NLRP3 inflammasome and expression of its downstream proteins.

Therefore, we hypothesized that EA, parecoxib, and EA + parecoxib treatments would reduce the inflammatory response by blocking the positive feedback of COX-2 to the NLRP3 inflammasome. NF-κB is required during the initiation phase to induce NLRP3 expression and constitutes the basis for NLRP3 inflammasome activation.[65,66] Therefore, a further possible mechanism underlying dysmenorrhea in PDM model rats may be COX-2-initiated activation of the signaling pathway. This induces NF-κB phosphorylation and translocation into the nucleus, NLRP3 inflammasome activation, and downstream release of the inflammatory factors IL-1 and IL-18. This ultimately results in uterine tissue damage and pain. Parecoxib sodium, targeting COX-2, inhibits the COX-2/NF-κB/NLRP3 signaling pathway and uterine inflammation in rats; hence, we hypothesized that the activation of the COX-2/NF-κB/NLRP 3 inflammatory signaling pathway is one of the pathological mechanisms involved in PDM. EA may downregulate the inflammatory response and alleviate pathological inflammatory damage in PDM model rats by inhibiting COX-2 expression, downregulating PG, and inhibiting the NF-κB signaling pathway and NLRP3 inflammasome activation. This impairs the NLRP3 inflammasome by effectively producing cleaved caspase-1, which interferes with IL-1β and IL-18 secretion. Therefore, the combination of EA and parecoxib sodium may exert anti-inflammatory effects.

We have conducted a multitude of studies focusing on the inflammatory mechanism of PMD and the anti-inflammatory mechanism of EA. Among these efforts, Liu et al[42] placed particular emphasis on exploring the impact of EA on NF-κB and NLRP3 inflammasomes within the uterine tissues of rats with PMD. Through rigorous experiments and in-depth analyses, they demonstrated that EA markedly ameliorates pain symptoms and alleviates pathological damage. Nevertheless, this research was mainly confined to investigating the mechanism by which EA influenced these inflammasomes, failing to conduct a profound dissection of the specific interaction relationship between EA and the NLRP3 signaling pathway. Tang et al[35] focused on MCC950 as an NLRP3 inflammasome inhibitor and examined the mechanism by which it alleviates PMD in mice through inhibiting the activation of NLRP3. The findings of their study robustly emphasized the crucial role of the NLRP3 pathway in the occurrence and development of PMD and also highlighted the potential value of inhibiting this pathway in reducing inflammatory responses. However, this study did not take EA into consideration. In contrast to these previous studies, the present study has taken a novel approach. We

have chosen the combined application of EA and parecoxib sodium as the entry point and have conducted an in-depth and comprehensive exploration into the comprehensive regulatory effect exerted by this combination on the COX-2/NF-κB/NLRP3 signaling pathway. We thus clearly revealed the unique regulatory pattern demonstrated by this combined application within this signaling pathway. Consequently, our research has opened up new avenues of thought and has provided fresh perspectives for the treatment of PMD. Hence, this treatment shows promising potential of playing an active and facilitating role in the optimization and improvement of subsequent treatment strategies for PMD.

Tang et al showed that MCC950 alleviated PDM in mice through the NF-κB/COX-2/PG pathway.[35] However, our study produced contrary results. This discrepancy can be attributed to several factors. First, we intraperitoneally injected parecoxib sodium to inhibit COX-2 expression. Second, we performed morphological observations, and the heterogeneity of the parameters could have introduced bias. Third, the complex inflammatory mechanisms induced by various drugs may have affected the results. COX-2 and NF-κB regulation may thus involve a complex bidirectional pathway, which remains to be confirmed.

Our results showed that the nuclear entry rate of NF-κB p65 decreased after electro-injection intervention. This indicated that electro-injection inhibited NF-κB nuclear entry, the expression of COX-2, p-NF-κBp65, NF-κBp65, and NLRP3 inflammasome and downstream factor protein was markedly reduced, uterine tissue PGF2α levels were considerably decreased, and PGE2 levels were notably increased. This indicates that the mechanism underlying EA intervention in PDM rats may involve the inhibition of COX-2 protein expression, NF-κBp65 phosphorylation into the nucleus, NF-κB protein expression, the NF-κB signal transduction pathway, expression of NLRP3 inflammasome activation, release of downstream IL-1 β and IL-18, prevention of inflammatory response and pathological damage in uterine tissues, and production of anti-inflammatory factors. Our results also showed that EA delayed or prevented the inflammatory response and pathological damage in the uterine tissue by regulating COX-2/NF-κB/NLRP3 signaling in PDM model rats.

This indicated that PDM-targeted EA exerted anti-inflammatory effects. Interestingly, EA + parecoxib suppressed the PDM inflammatory response through synergistic anti-inflammatory mechanisms. To the best of our knowledge, this is the first study to report such findings regarding EA and parecoxib combination therapy for PDM. Indeed, EA + parecoxib showed stronger effects on COX-2/NF-κB/NLRP 3 signaling pathway-related proteins than that of EA or parecoxib administration alone.

The results of this study showed that electrical impulses have anti-inflammatory effects in PDM rats. EA regulated the COX-2/NF-κB/NLRP3 signaling pathway and delayed, or prevented, the inflammatory response and pathological damage of uterine tissue. This provides a potential new treatment option for menstrual pain and an alternative to exclusive treatment with drugs, such as ibuprofen and parecoxib sodium. This study also revealed that the combination of EA with parecoxib sodium may produce a synergistic therapeutic effect in PDM.

Our study has multiple strengths, including the use of a well-established PDM rat model and the comprehensive analysis of both histopathological and molecular changes. The combination of behavioral, histological, and ultrastructural assessments provides a robust evaluation of the effects of EA and parecoxib on PDM. Additionally, the use of TEM allows for the detailed examination of cellular changes, providing valuable insights into the mechanisms underlying the observed anti-inflammatory effects.

After the oxytocin-induced PDM model was established,[8,35,67] the rats exhibited notable writhing responses, and the levels of the pro-inflammatory factor $PGF_{2\alpha}$ increased. These results indicate that oxytocin predominantly exerted a pro-inflammatory effect under the specified experimental conditions, thereby successfully inducing dysmenorrhea-like symptoms and validating the effectiveness of the model in simulating clinical dysmenorrhea. This aligns with the study's objectives and outcomes, and our findings confirm the pro-inflammatory role of oxytocin in acute PDM modeling. Interestingly, recent studies suggest that oxytocin may also exert anti-inflammatory effects.[68] To further clarify the mechanism of action of oxytocin in the model used in the present study, subsequent experiments should involve setting different oxytocin dosage groups to thoroughly assess their dynamic impacts on inflammation and uterine contractions. By building on the existing model, this approach will continuously refine and optimize the PMD modeling system, thereby facilitating a more comprehensive and accurate elucidation of relevant physiological and pathological mechanisms.

There are also limitations that should be addressed in future research. We used histology, protein blotting, and ELISA to determine protein expression but did not detect changes among factors at the gene level. Furthermore, we did not isolate uterine cells to explore the precise regulatory mechanisms. While our findings suggest that EA and parecoxib can effectively reduce inflammatory injury in the short term, longer-term studies are needed to determine the sustained effects of these treatments. Additionally, while our findings suggest a potential mechanism involving the COX-2/NF-κB/NLRP3 pathway, further studies are needed to confirm this and to elucidate the precise molecular interactions involved.

Conclusion

In this study, we demonstrated the involvement of the COX-2/NF-κB/NLRP3 signaling pathway in the development of the inflammatory response in PDM and that COX-2 may be a potential target for PDM treatment. Parecoxib sodium, which targets COX-2, may have inhibited this signaling pathway in rats, thereby reducing uterine inflammation. EA delayed or prevented inflammatory responses and pathological damage of uterine tissue, likely by regulating this pathway, which suggests anti-inflammatory effects of electro-targeting in PDM model rats. The novel finding that inhibiting the COX-2 signaling pathway reduces the release of inflammatory mediators in PDM provides novel insights into the pathogenesis of PDM and will help facilitate the identification of novel therapeutic targets. Furthermore, EA inhibition of COX-2 is a potential new direction for future treatment of PDM and an alternative to ibuprofen. The combination of EA with parecoxib markedly inhibited the release of inflammatory factors, which emphasizes the potential use of acupuncture combined with drug treatments to inhibit PDM-associated inflammation and reduce the side effects of NSAIDs. This combination of anti-inflammatory therapies may be a potential therapeutic strategy against PDM.

Abbreviations

PDM, primary dysmenorrhea; EA, electroacupuncture; COX-2, cyclooxygenase-2; NF-κB, nuclear factor kappa B; NLRP3, nucleotide-binding oligomerization domain-like receptor protein 3; ASC, apoptosis-associated speck-like protein; pro-caspase-1, pro-cysteine aspartic acid-specific protease 1; caspase-1, cysteine aspartic acid-specific protease 1; IL, interleukin; PG, prostaglandin; PGE2, prostaglandin E2; PGF2α, prostaglandin F2α; ELISA, enzyme-linked immunosorbent assay; HE, hematoxylin and eosin; TEM, transmission electron microscopy; NF-κBp65, nuclear transcription factor p65; AI, artificial intelligence; ER, endoplasmic reticulum; CFs, collagen fibers.

Data Sharing Statement

The minimal data set underlying the results described in our manuscript are available in the Supporting Information and in a public data repository (https://figshare.com/articles/dataset/_zip/24716895).

Ethics Approval and Informed Consent

The study protocol was approved by the Institutional Animal Care and Use Committee of Hunan University of Traditional Chinese Medicine (protocol number LL2021040703). We have read and understood your journal's policies and believe that neither the manuscript nor the study violates any of these.

Consent for Publication

This manuscript has not been published or presented elsewhere in part or in entirety and is not under consideration by another journal.We, the authors, confirm that appropriate consent has been obtained for all materials (images, videos, etc.) used in this manuscript. Participants were informed of the study and consented to publication. We have already uploaded the signed consent forms by all authors as required during the submission process.

Acknowledgments

We extend our gratitude to all researchers involved in the study for their invaluable assistance and efforts. We also thank Editage (www.editage.cn) for providing professional English language editing services.

Author Contributions

All authors made a significant contribution to the work reported, whether that is in the conception, study design, execution, acquisition of data, analysis and interpretation, or in all these areas; took part in drafting, revising or critically reviewing the article; gave final approval of the version to be published; have agreed on the journal to which the article has been submitted; and agree to be accountable for all aspects of the work.

Funding

This work was supported by the Youth Program of National Natural Science Foundation of China (NSFC,No. 82004490), https://grants.nsfc.gov.cn/; the Hunan Natural Science Foundation Youth Foundation project (No.2023JJ40598), https://www.usc.edu.cn/; the Health Research Project of Hunan Provincial Health Commission (No. W20243177), https://hunan.wsglw.net/HomePublic/PublicIndex; the Outstanding Youth Project of Hunan Provincial Department of Education (No. 24B0428), http://jyt.hunan.gov.cn/., and the University of South China Clinical Research 4310 Program (No. 20214310NHYCG04); https://yjs.usc.edu.cn/.(S4 Appendix). The funders had and will not have a role in study design, data collection and analysis, decision to publish, or preparation of the manuscript.

Disclosure

The authors report no conflicts of interest in this work.

References

1. ACO N. 760 summary: dysmenorrhea and endometriosis in the adolescent. *Obstet Gynecol*. 2018.
2. Burnett M, Lemyre M. 345-primary dysmenorrhea consensus guideline. *J Obstet Gynaecol Can*. 2017;39:585–95.
3. Kho KA, Shields JK. Diagnosis and management of primary dysmenorrhea. *JAMA*. 2020;323(3):268–269.
4. Bancroft J, Rennie D, Warner P. Vulnerability to perimenstrual mood change: the relevance of a past history of depressive disorder. *Psychosom Med*. 1994;56(3):225–231. doi:10.1097/00006842-199405000-00008
5. Häuser W, Schmutzer G, Brähler E. Prevalence of disabling abdominal pain and menstrual cramp. Results from a representative survey of the general German population. *Schmerz*. 2014;28(3):259–264. doi:10.1007/s00482-014-1404-8
6. Meng L, Li J, Cheng Y, et al. Dysmenorrhea increased the risk of postpartum depression in Chinese Han parturients. *Sci Rep*. 2019;9(1):16579. doi:10.1038/s41598-019-53059-8
7. Yasir S, Kant B, Dar MF. Frequency of dysmenorrhoea, its impact and management strategies adopted by medical students. *J Ayub Med Coll Abbottabad*. 2014;26(3):349–352.
8. Yang L, Cao Z, Yu B, Chai C. An in vivo mouse model of primary dysmenorrhea. *Exp Anim*. 2015;64(3):295–303. doi:10.1538/expanim.14-0111
9. Iacovides S, Avidon I, Baker FC. What we know about primary dysmenorrhea today: a critical review. *Hum Reprod Update*. 2015;21(6):762–778. doi:10.1093/humupd/dmv039
10. Wouters E, Hudson CA, McArdle CA, Bernal AL. Central role for protein kinase C in oxytocin and epidermal growth factor stimulated cyclooxygenase 2 expression in human myometrial cells. *BMC Res Notes*. 2014;7:357. doi:10.1186/1756-0500-7-357
11. Hayden MS, Ghosh S. NF-κB, the first quarter-century: remarkable progress and outstanding questions. *Genes Dev*. 2012;26:203–34.
12. Khalfallah M, Allaithy A, Maria DA. Incidence, predictors and outcomes of contrast induced nephropathy in patients with ST elevation myocardial infarction undergoing primary percutaneous coronary intervention. *Glob Heart*. 2021;16(1):57. doi:10.5334/gh.1071
13. Li KZ, Liao ZY, Li YX, et al. A20 rescues hepatocytes from apoptosis through the NF-κB signaling pathway in rats with acute liver failure. *Biosci Rep*. 2019;39(1). doi:10.1042/BSR20180316
14. Gajtkó A, Bakk E, Hegedűs K, Ducza L, Holló K. IL-1β induced cytokine expression by spinal astrocytes can play a role in the maintenance of chronic inflammatory pain. *Frontiers in Physiology*. 2020;11:543331.
15. Pilat D, Piotrowska A, Rojewska E. Blockade of IL-18 signaling diminished neuropathic pain and enhanced the efficacy of morphine and buprenorphine. *Mol Cell Neurosci*. 2016;71:114–24.
16. Broz P, von Moltke J, Jones JW, et al. Differential requirement for Caspase-1 autoproteolysis in pathogen-induced cell death and cytokine processing. *Cell Host Microbe*. 2010;8(6):471–483. doi:10.1016/j.chom.2010.11.007
17. Yu SY, Li XL. Pyroptosis and inflammasomes in obstetrical and gynecological diseases. *Gynecol Endocrinol*. 2021;37:385–91.
18. Hu X, Li D, Wang J, et al. Melatonin inhibits endoplasmic reticulum stress-associated TXNIP/NLRP3 inflammasome activation in lipopolysaccharide-induced endometritis in mice. *Int Immunopharmacol*. 2018;64:101–109. doi:10.1016/j.intimp.2018.08.028
19. Bi W, Cheng X, Zeng Z, et al. Rifampicin ameliorates lipopolysaccharide-induced cognitive and motor impairments via inhibition of the TLR4/MyD88/NF-κB signaling pathway in mice. *Neurol Res*. 2021;2021:1–14.
20. Zhang LY, Zhan DL, Chen YY, et al. Aflatoxin B1 enhances pyroptosis of hepatocytes and activation of Kupffer cells to promote liver inflammatory injury via dephosphorylation of cyclooxygenase-2: an in vitro, ex vivo and in vivo study. *Arch Toxicol*. 2019;93(11):3305–3320.
21. Hua KF, Chou JC, Ka SM, et al. Cyclooxygenase-2 regulates NLRP3 inflammasome-derived IL-1β production. *J Cell Physiol*. 2015;230(4):863–874. doi:10.1002/jcp.24815
22. Liu R, Wu S, Guo C, et al. Ibuprofen exerts antiepileptic and neuroprotective effects in the rat model of pentylenetetrazol-induced epilepsy via the COX-2/NLRP3/IL-18 pathway. *Neurochem Res*. 2020;45(10):2516–2526. doi:10.1007/s11064-020-03109-9

23. Yang HH, Duan JX, Liu SK, et al. A COX-2/sEH dual inhibitor PTUPB alleviates lipopolysaccharide-induced acute lung injury in mice by inhibiting NLRP3 inflammasome activation. *Theranostics*. 2020;10(11):4749–4761. doi:10.7150/thno.43108
24. Yu WY, Ma LX, Zhang Z, et al. Acupuncture for primary dysmenorrhea: a potential mechanism from an anti-inflammatory perspective. *Evid Based Complement Alternat Med*. 2021;2021:1907009. doi:10.1155/2021/1907009
25. Yang NN, Yang JW, Ye Y, et al. Electroacupuncture ameliorates intestinal inflammation by activating α7nAChR-mediated JAK2/STAT3 signaling pathway in postoperative ileus. *Theranostics*. 2021;11(9):4078–4089.
26. Liu S, Wang Z, Su Y, et al. A neuroanatomical basis for electroacupuncture to drive the vagal-adrenal axis. *Nature*. 2021;598(7882):641–645. doi:10.1038/s41586-021-04001-4
27. Biao T, Dan L, Lingyu C, Liu Y. NLRP3 inflammasome inhibitor MCC950 attenuates primary dysmenorrhea in mice via the NF-κB/COX-2/PG pathway. *J Inflamm*. 2020;17(1):1–9.
28. Liu Y, Wang Y, Chen L, et al. Effect of electroacupuncture on NF-κB and NLRP3 inflammasome in uterine tissues of rats with primary dysmenorrhea. *Journal of Acupuncture and Tuina Science*. 2019;17(4). doi:10.1007/s11726-019-1117-8
29. Xie Y, Qian J, Lu Q. The therapeutic effect of ge-gen decoction on a rat model of primary dysmenorrhea: label-free quantitative proteomics and bioinformatic analyses. *Biomed Res Int*. 2020;2020:5840967. doi:10.1155/2020/5840967
30. Hwang YC, Lee IS, Ryu Y, Lee MS, Chae Y. Exploring traditional acupuncture point selection patterns for pain control: data mining of randomised controlled clinical trials. *Acupunct Med*. 2020;964528420926173. doi:10.1177/0964528420926173
31. Wang S, Yuan H, Li J, et al. Effect of electroacupuncture on NLRP3 inflammasome and morphology of uterine in rats with primary dysmenorrhea based on meridian acupoint viscera correlation theory. *World Journal of Traditional Chinese Medicine*. 2023;9(02):123–130.
32. Wei Y, Ma T, Wang H, et al. Extracts of compound Muniziqi granule suppressed uterus contraction and ameliorated oxytocin-induced primary dysmenorrhea. *J Ethnopharmacol*. 2018;223:33–40. doi:10.1016/j.jep.2018.05.024
33. Wei A, Feng H, Jia XM, Tang H, Liao YY, Li BR. Ozone therapy ameliorates inflammation and endometrial injury in rats with pelvic inflammatory disease. *Biomed Pharmacother*. 2018;107:1418–25.
34. Böttcher B, Laterza RM, Wildt L, et al. A first-in-human study of PDC31 (prostaglandin F2α receptor inhibitor) in primary dysmenorrhea. *Hum Reprod*. 2014;29:2465–73.
35. Tang B, Liu D, Chen L, Liu Y. NLRP3 inflammasome inhibitor MCC950 attenuates primary dysmenorrhea in mice via the NF-κB/COX-2/PG pathway. *J Inflamm*. 2020;17:22. doi:10.1186/s12950-020-00251-7
36. Murata T, Narita K, Ichimaru T. Rat uterine oxytocin receptor and estrogen receptor α and β mRNA levels are regulated by estrogen through multiple estrogen receptors. *J Reprod Dev*. 2014;60(1):55–61. PMID: 24334513. doi:10.1262/jrd.2012-139
37. Luca AM, Carvalho J, Ramachandran N, Balki M. The effect of morbid obesity or advanced maternal age on oxytocin-induced myometrial contractions: an in vitro study. *Can J Anaesth*. 2020;67(7):836–846. PMID: 32189217. doi:10.1007/s12630-020-01615-6
38. Li M, Bi J, Lv B, et al. An experimental study of the anti-dysmenorrhea effect of Chinese herbal medicines used in Jin Gui Yao Lue. *J Ethnopharmacol*. 2019;245:112181. doi:10.1016/j.jep.2019.112181
39. Hulls CM, Lentle RG, Chua WH, et al. Spatiotemporal mapping of the contracting gravid uterus of the rabbit shows contrary changes with increasing gestation and dosage with oxytocin. *Front Endocrinol*. 2019;10:802. doi:10.3389/fendo.2019.00802
40. Sun L, Liu L, Zong S, et al. Traditional Chinese medicine Guizhi Fuling capsule used for therapy of dysmenorrhea via attenuating uterus contraction. *J Ethnopharmacol*. 2016;191:273–279. doi:10.1016/j.jep.2016.06.042
41. Ferries-Rowe ECE, Archer JS, Archer JS. Primary dysmenorrhea: diagnosis and therapy. *Obstet Gynecol*. 2020;136(5):1047–1058. doi:10.1097/AOG.0000000000004096
42. Zhang H, Liu X, Jiang H, Liu Z, Zhang XY, Xie HZ. Parecoxib increases muscle pain threshold and relieves shoulder pain after gynecologic laparoscopy: a randomized controlled trial. *J Pain Res*. 2016;9:653–660. doi:10.2147/JPR.S115889
43. de Almeida JL, Jukemura J, Coelho AM, Patzina RA, Machado MC, da Cunha JE. Inhibition of cyclooxygenase-2 in experimental severe acute pancreatitis. *Clinics*. 2006;61(4):301–306. doi:10.1590/S1807-59322006000400005
44. Colanardi MC, Nettis E, Traetta P, et al. Safety of parecoxib in patients with nonsteroidal anti-inflammatory drug-induced urticaria or angioedema. *Ann Allergy Asthma Immunol*. 2008;100(1):82–85. doi:10.1016/S1081-1206(10)60409-7
45. Vadalouca A, Moka E, Chatzidimitriou A. Effect on anxiety levels and procedural pain during epidural catheter placement for surgical opera- tions or for chronic pain therapy. *Pain Pract*.2009;9:181–94.
46. Wang RD, Zhu JY, Zhu Y, Ge YS, Xu GL, Jia WD. Perioperative analgesia with parecoxib sodium improves postoperative pain and immune function in patients undergoing hepatectomy for hepatocellular carcinoma. *J Eval Clin Pract*. 2020;26(3):992–1000. doi:10.1111/jep.13256
47. Li P, Zheng X, Wu Y, Peng J. The efficacy of parecoxib for pain control after hysterectomy: a meta-analysis of randomized controlled studies. *J Matern Fetal Neonatal Med*. 2021;34(21):3488–3495. doi:10.1080/14767058.2019.1685972
48. Becker A, Geisslinger G, Murín R, et al. Cannabinoid-mediated diversity of antinociceptive efficacy of parecoxib in Wistar and Sprague Dawley rats in the chronic constriction injury model of neuropathic pain. *Naunyn Schmiedebergs Arch Pharmacol*. 2013;386(5):369–382. doi:10.1007/s00210-013-0839-2
49. Ayar A. Tocolytic effect of parecoxib, a new parenteral cyclo-oxygenase-2-specific inhibitor, on the spontaneous and prostaglandin-induced contractions of rat isolated myometrium. *Clin Exp Pharmacol Physiol*. 2007;34(8):737–741. doi:10.1111/j.1440-1681.2007.04632.x
50. Marjoribanks J, Ayeleke RO, Farquhar C, et al. Nonsteroidal anti-inflammatory drugs for dysmenorrhoea. *Cochrane Database Syst Rev*. 2015;2015(7):CD001751. doi:10.1002/14651858.CD001751.pub3
51. Shin D, Lee SJ, Ha YM, et al. Pharmacokinetic and pharmacodynamic evaluation according to absorption differences in three formulations of ibuprofen. *Drug Des Devel Ther*. 2017;11:135–141. doi:10.2147/DDDT.S121633
52. Orlando BJ, Lucido MJ, Malkowski MG. The structure of ibuprofen bound to cyclooxygenase-2. *J Struct Biol*. 2015;189(1):62–66. doi:10.1016/j.jsb.2014.11.005
53. Xia MQ, Tian CL, Liu L, Hu RF, Gui SY, Chu XQ. Transdermal administration of ibuprofen-loaded gel: preparation, pharmacokinetic profile, and tissue distribution. *AAPS PharmSciTech*. 2020;21(3):84. doi:10.1208/s12249-020-1627-1
54. Marjoribanks J, Proctor ML, Farquhar C. Nonsteroidal anti-inflammatory drugs for primary dysmenorrhoea. *Cochrane Database Syst Rev*. 2003;4:CD001751. doi:10.1002/14651858.CD001751

55. Irvine J, Afrose A, Islam N. Formulation and delivery strategies of ibuprofen: challenges and opportunities. *Drug Dev Ind Pharm*. 2018;44 (2):173–183. doi:10.1080/03639045.2017.1391838
56. Swanson KV, Deng M, Ting JP. The NLRP3 inflammasome: molecular activation and regulation to therapeutics. *Nat Rev Immunol*. 2019;19:477–89.
57. Li Y, Liu M, Zuo Z, et al. TLR9 regulates the NF-κB-NLRP3-IL-1β pathway negatively in Salmonella-induced NKG2D-Mediated intestinal inflammation. *The J Immunol*. 2017;199(2):761–773. doi:10.4049/jimmunol.1601416
58. Pontillo A, Bricher P, Leal VN, Lima S, Souza PR, Crovella S. Role of inflammasome genetics in susceptibility to HPV infection and cervical cancer development. *J Med Virol*. 2016;88(9):1646–1651. doi:10.1002/jmv.24514
59. Zhao G, Jiang K, Yang Y, et al. The potential therapeutic role of miR-223 in bovine endometritis by targeting the NLRP3 inflammasome. *Front Immunol*. 2018;9:1916. doi:10.3389/fimmu.2018.01916
60. Zhao P, Fu H, Cheng H, et al. Acupuncture at ST36 alleviates the behavioral disorder of autistic rats by inhibiting TXNIP-mediated activation of NLRP3. *J Neuropathol Exp Neurol*. 2022;81(2):127–134. doi:10.1093/jnen/nlab132
61. Li X, Wang H, Li C, et al. Acupuncture inhibits NLRP3 inflammasome activation in the prefrontal cortex of a chronic stress rat model of depression. *Anat Rec*. 2021;304(11):2470–2479. doi:10.1002/ar.24778
62. Mokhtari T, Yue LP, Hu L. Exogenous melatonin alleviates neuropathic pain-induced affective disorders by suppressing NF-κB/ NLRP3 pathway and apoptosis. *Sci Rep*. 2023;13(1):2111. PMID: 36747075. doi:10.1038/s41598-023-28418-1
63. Sun L, Yong Y, Wei P, et al. Electroacupuncture ameliorates postoperative cognitive dysfunction and associated neuroinflammation via NLRP3 signal inhibition in aged mice. *CNS Neurosci Ther*. 2021;s:1.
64. Zhang J, Yang X, Zhang X, et al. Electro-acupuncture protects diabetic nephropathy-induced inflammation through suppression of NLRP3 inflammasome in renal macrophage Isolation. *Endocr Metab Immune Disord Drug Targets*. 2021;21(11):2075–2083. doi:10.2174/1871530321666210118161721
65. Shen C, Zhang Z, Xie T, et al. Rhein suppresses lung inflammatory injury induced by human respiratory syncytial virus through inhibiting NLRP3 inflammasome activation via NF-κB pathway in mice. *Front Pharmacol*. 2019;10:1600. doi:10.3389/fphar.2019.01600
66. Yin N, Gao Q, Tao W, et al. Paeoniflorin relieves LPS-induced inflammatory pain in mice by inhibiting NLRP3 inflammasome activation via transient receptor potential vanilloid 1. *J Leukoc Biol*. 2020;108(1):229–241. doi:10.1002/JLB.3MA0220-355R
67. Hong F, He G, Zhang M, Yu B, Chai C. The establishment of a mouse model of recurrent primary dysmenorrhea. *Int J Mol Sci*. 2022;23(11):6128. doi:10.3390/ijms23116128
68. Friuli M, Eramo B, Valenza M, Scuderi C, Provensi G, Romano A. Targeting the oxytocinergic system: a possible pharmacological strategy for the treatment of inflammation occurring in different chronic diseases. *Int J Mol Sci*. 2021;22(19):10250. doi:10.3390/ijms221910250